Hindawi
Shock and Vibration
Volume 2022, Article ID 2814807, 16 pages
https://doi.org/10.1155/2022/2814807

Research Article

Study on the Vertical Stiffness of Bridge Expansion Joints Based on the Vehicle-Track-Bridge Coupled Model

Yunlu Wang,[1] **Mangmang Gao**,[2] **and Fei Yang**[2]

[1]*China Academy of Railway Sciences, Beijing 100081, China*
[2]*Infrastructure Inspection Research Institute, China Academy of Railway Sciences Corporation Limited, Beijing 100081, China*

Correspondence should be addressed to Mangmang Gao; vanillaw1995@163.com

Received 13 January 2022; Revised 5 May 2022; Accepted 20 May 2022; Published 11 July 2022

Academic Editor: Iacopo Tamellin

Copyright © 2022 Yunlu Wang et al. This is an open access article distributed under the Creative Commons Attribution License, which permits unrestricted use, distribution, and reproduction in any medium, provided the original work is properly cited.

Bridge expansion joints (BEJs) are equipped at the girder end of long-span railway bridges to ensure the reliable transition of the track. BEJs should have suitable dynamic stiffness to ensure the running safety and stability of the vehicle. To explore the influence of dynamic vertical stiffness of BEJs on the dynamic response of vehicle, track, and bridge, a three-dimensional vehicle-track-bridge coupled model is established, and the influence of sleeper spacing and vehicle speed are taken into consideration. Taking a high-speed railway line in China as a case study, the dynamic response of the whole system is calculated. The results show that (1) the dynamic response of BEJs and the vehicle is affected by the vehicle speed and sleeper spacing. With the increase of vehicle speed and sleeper spacing, the dynamic response of the system increases; (2) the vertical stiffness of BEJs will affect the dynamic response of BEJs and the interaction between the wheel and rail: the vertical dynamic displacement of movable sleeper will exceed the limit if the vertical stiffness of pressure-bearing is insufficient, and the wheel unloading rate may exceed the limit if the vertical stiffness of the cushion plate is insufficient. Based on the results, the larger vertical stiffness of the cushion plate and pressure-bearing is recommended. These results have been applied to the design of BEJs on the studied railway line, which are in good service condition at present.

1. Introduction

Nowadays, bridges are widely used in high-speed railway (HSR) to provide stable and easy maintenance line conditions [1, 2]. Vehicle, track, and bridge constitute a coupled system [3, 4], and the running safety and stability of the vehicle will be affected by the track and bridge [5, 6].

Researchers have conducted a lot of work about the vehicle-track-bridge coupled system. Zhang [7] proposed an analysis method based on the pseudo-excitation method for the vehicle-bridge interaction system and obtained the probability density functions for safety factors and the probabilities of safety factors exceeding the given limits. Gao [1] proposed a vehicle-track-bridge coupled analysis method based on forced vibration, pointing out that local fastener failure will slightly affect the vibration of the track and carbody, but it will significantly intensify the interaction between wheel and rail. Jiang [8] used the new point estimate method to analyze the random dynamic responses of the 3D train-bridge coupled system with random parameters. Gong [9] studied the influence of spatially varying ground motion on the dynamic behavior of a train passing through a cable-stayed bridge. Xiang [10] investigated the influence of the track irregularity and deck deformation on the running safety of HSR trains. Chen [11] studied the influence of track stiffness on dynamic behaviors of the high-speed vehicle-track-bridge dynamic system. However, few studies have focused on the impact of the ancillary structure of the bridge on the vehicle-track-bridge coupled system.

With the increasing bridge span, BEJs have become a vital device for long-span railway bridges. It is not only required to match the deformation of the girder end but also required to have enough strength and stiffness to bear the dynamic load brought by the vehicle. Since the track structure in BEJs is very different from that on the bridge, and the BEJs lack the support of lower foundation, BEJs are

regarded as the weak parts of the railway and have attracted extensive interest from researchers. The performance of BEJs, including the static deformation and joint force, in service condition have been studied [12–15], and plenty of work has been conducted on the failure mechanism of BEJs [16, 17]. Since the track irregularity in BEJs can only be reduced by adjusting the height of the plate under the rail, and the adjustment range of height is very small, the deformation of BEJs should be controlled. The increase of stiffness of BEJs can reduce the deformation of the structure, but it will weaken the elasticity of the structure. Moreover, the vertical stiffness of BEJs should not differ too much from that of girders on both sides. The excessive change of track stiffness is unfavorable to running safety of the vehicle. Therefore, the stiffness of BEJs should be adopted reasonably. This study aims to provide a theoretical basis for adopting the stiffness of BEJs by analyzing the dynamic response of the vehicle and BEJs.

Taking a high-speed railway line in China as a case to study, it has a total length of about 314 km, and the design speed of the vehicle is 250 km/h. In order to reduce the seismic response of the structure, hyperboloid bearings are used as seismic isolation devices for bridges, which results in a large displacement of the girder end. As the result, this railway line is equipped with BEJs at many positions to ensure the continuity of the track structure. The layout scheme of BEJs is shown in Figure 1. The short vertical line represents the position of BEJs, and the passing time of the vehicle is also marked in the figure. As highlighted in the dashed box, the vehicle passes through the section with the densest arrangement of BEJs within 7.8 s.

In order to avoid the interference of boundary conditions, and consider the continuous impact of densely arranged BEJs on the vehicle, the section in the dashed box of Figure 1 is studied rather than only analyzing one BEJ. The vehicle-track-bridge coupled model is established to investigate the influence of vertical stiffness of BEJs on the whole system by considering the influence of different displacement of the girder end and different vehicle speed. The dynamic response of the vehicle and BEJs is calculated when the vehicle passes through this section and evaluated based on the code. This study clarified the influence of BEJs' parameters on the dynamic response of the vehicle-track-bridge coupled system, and provided the suggestion of the reasonable value of vertical stiffness of BEJs based on the results.

2. Numerical Model

2.1. Bridge Model. The studied section includes two bridge structures: (A) 32 m precast post-tensioned prestressed concrete simply supported box girder; (B) a $60\,m + 100\,m + 60$ m prestressed concrete double track continuous girder. MIDAS is used to establish the finite element model (FEM) of the bridge, as shown in Figure 2, while the arrowhead indicates the forward direction of the vehicle. The boxes mark the positions of BEJs.

The bridges are simulated by beam elements. The bottom of the pier is fixed, and the constraints between the pier and

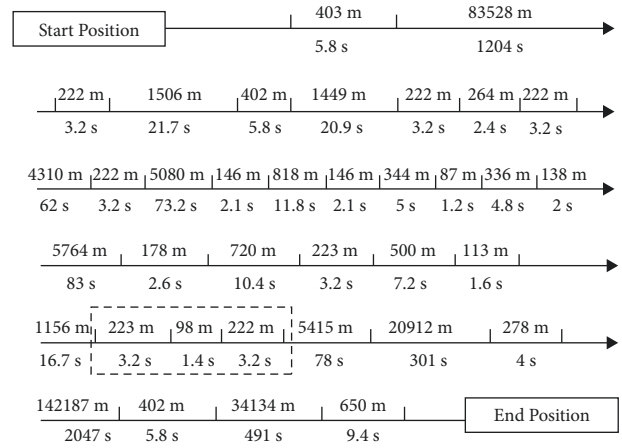

Figure 1: Layout scheme of BEJs in the high-speed railway line.

the bridge deck are simulated by master-slave nodes. And the secondary dead load is applied to the girder body by increasing the bulk density of materials. Because the concrete bridge will arch due to the creep, which will influence the running stability of the vehicle [10, 18], the creep is taken as the initial deformation of the bridge deck in the model. The uniform stiffness matrix and the uniform mass matrix are adopted in dynamic analysis with Rayleigh damping.

The motion equation of the bridge is shown in equation (1), where $[M_b]$, $[C_b]$, and $[K_b]$ is the mass, damping, and stiffness matrix of the bridge, respectively; $\{X_b\}$ represents the displacement vector of the bridge; $\{P_{bt}\}$ is the interaction force between the track and the bridge, which is the function of the displacement and velocity of the track and the bridge.

$$[M_b]\{\ddot{X}_b\} + [C_b]\{\dot{X}_b\} + [K_b]\{X_b\} = \{P_{bt}\}. \quad (1)$$

2.2. BEJs Model. BEJs with sliding sleeper is applied in the railway bridge studied. The structure of this type of BEJs is simpler than other styles, which is less affected by the displacement of the girder end and can be applied to the condition with a wider range of vehicle speed. The structure of BEJs is shown in Figure 3. It is mainly composed of fixed steel sleeper 2, movable steel sleeper 3, supporting frame 7, supporting beam 4, cushion plate 5 (between fixed sleepers and supporting frames), connecting rods 6, and pressure-bearing 8 (between supporting beams and sleepers). The rail and concrete sleeper are denoted in the figure 1 and 9, respectively.

The supporting frames are installed on the girder body and have no relative displacement with the bridge. The fixed sleepers and supporting frames are connected by bolts, and there are no longitudinal and lateral relative displacements between them. The local vertical stiffness is provided by the cushion plates between them. One end of the supporting beam is connected with fixed sleepers, and fixed sleepers at the other end and the movable sleeper can slide relative to the supporting beam in the longitudinal direction. There is no lateral relative displacement between supporting beams and sleepers, and the local vertical stiffness is provided by the

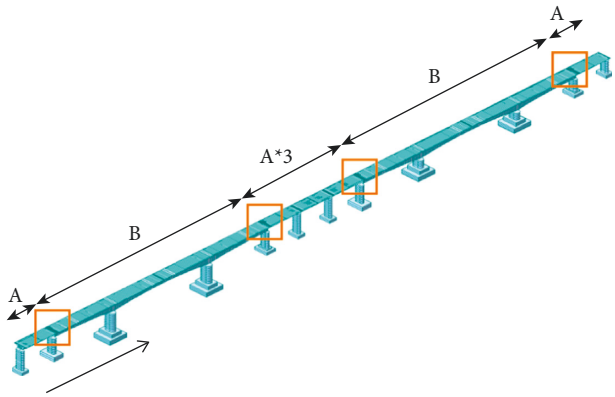

Figure 2: The MIDAS model of the bridge.

pressure-bearings between them. The movable steel sleeper, which suspended on the supporting beam, is connected to fixed sleepers through connecting rods. When longitudinal displacement occurs at the girder end, fixed sleepers at the one end and the movable sleeper slide relative to the supporting beam, and sleeper spacing between fixed sleepers and movable sleepers are adjusted by connecting rods. The maximum longitudinal displacement of girder ends on both sides of BEJs is ±200 mm. The distance between the fixed sleeper and the movable sleeper is 450 mm when the longitudinal displacement of the girder end is 0 mm, and which is 350 mm or 550 mm when the longitudinal displacement of the girder end is +200 mm or -200 mm, respectively.

The vertical stiffness of BEJs should not differ too much from that of girders on both sides. In order to make the stiffness under the sleeper of BEJs consistent with the stiffness under the sleeper of the ballasted track, the cushion plate is placed under the fixed steel sleeper. By adjusting the stiffness of the cushion plate, the abrupt change of track stiffness can be avoided, which is unfavorable to the running safety and stability. The pressure-bearing is placed between the sleepers and supporting beams to adjust the stiffness of BEJs too. The range of vertical stiffness of the cushion plate is 80 ~ 120 kN/mm, and the range of vertical stiffness of the pressure-bearing is 160 ~ 240 kN/mm.

BEJs are modeled as the substructures of the bridge model through MIDAS, as shown in Figure 4. Since the supporting frame are fixed with the bridge deck, it can be ignored in the model. The supporting beam and sleepers are simulated by beam elements, which are denoted in the figure. The nonlinear characteristics of track stiffness have little influence on the results and cost plenty of computational resources [19], hence, linear massless spring elements are used to simulate cushion plates and pressure-bearings. The stiffness of the spring in the BEJs model are changed to simulate different stiffness of cushion plates and pressure-bearings. And the MIDAS model of BEJs with different sleeper spacing is established to consider the influence of longitudinal displacement of the girder end on the system. Table 1 lists the details of different cases.

Figure 5 shows the top view of BEJ models with different sleeper spacing, which is 350 mm, 450 mm, and 550 mm, respectively.

2.3. Vehicle Model. The vehicle model consists of 16 vehicles with 8 electric moto units (EMUs), which are composed of car-bodies, bogies, wheelsets, and the spring and damping connections. In order to simplify the calculation, the mechanics model of the vehicle adopts the following assumptions [4, 20–22]: (1) the car-bodies, bogies, and wheelsets are regarded as rigid components, the connections are represented by linear spring and linear damping. (2) The vehicles move at constant speed along the track, the influence of the longitudinal force of the system is ignored. (3) The wheelsets are always in contact with the rail.

As shown in Figure 6, the vehicle is modeled by multibody mechanics with 23 degrees of freedom (DOF). The car-body has 5 DOF to be concerned: lateral displacement Y_c, vertical displacement Z_c, roll angle θ_c, yaw angle Ψ_c, and pitch angle φ_c. The bogie has 5 DOF too, which is denoted by subscript t. And the lateral displacement and roll angle of wheelsets are considered, which is denoted by subscript w. Table 2 provides the main parameters of the vehicle model.

The motion equation of the vehicle is shown in equation (2), where $[M_v]$, $[C_v]$, and $[K_v]$ are the mass, damping, and stiffness matrix of the vehicle, respectively; $\{X_v\}$ represents the displacement vector of the vehicle; $\{P_{wr}\}$ is the wheel-rail interaction force, which is the function of the displacement and velocity of the vehicle and the rail. The lateral wheel-rail interaction force is derived from the Kalker creep theory, and the vertical wheel-rail interaction force is obtained according to the static balance condition of the wheelsets.

$$[M_v]\{\ddot{X}_v\} + [C_v]\{\dot{X}_v\} + [K_v]\{X_v\} = \{P_{wr}\}. \quad (2)$$

2.4. Track Model. The rail is modeled by the finite element method, and the under-rail structure is simulated by mass-spring-dashpot models. The parameters of the ballasted track are provided by Table 3 [19]. The vertical stiffness of ballast is 9.50×10^7 N/m, which is the measured data of Jinan Yellow River bridge. In order to investigate the most unfavorable conditions, the track arranged near the outside of the bridge deck.

The motion equation of the track is shown in equation (3), where $[M_t]$, $[C_t]$, and $[K_t]$ are the mass, damping, and stiffness matrices of the track, respectively; $\{X_t\}$ represents the displacement vector of the track; the external load acting on the track includes two parts: the wheel-rail force and the interaction force between the track and the bridge. The force of the bridge acting on the track is calculated by forced vibration [1].

$$[M_t]\{\ddot{X}_t\} + [C_t]\{\dot{X}_t\} + [K_t]\{X_t\} = \{P_{wr}\} + \{P_{bt}\}. \quad (3)$$

2.5. Track Irregularity. The track irregularity samples used in this study are generated by power spectral density (PSD) of rail irregularity of high-speed railway lines in German [23], the length of the sample is 1000 m and the range of the wavelength is 1m ~ 80 m.

The track irregularity is expressed as equation (4), where S_v, S_a, and S_c denote the PSD of height irregularity,

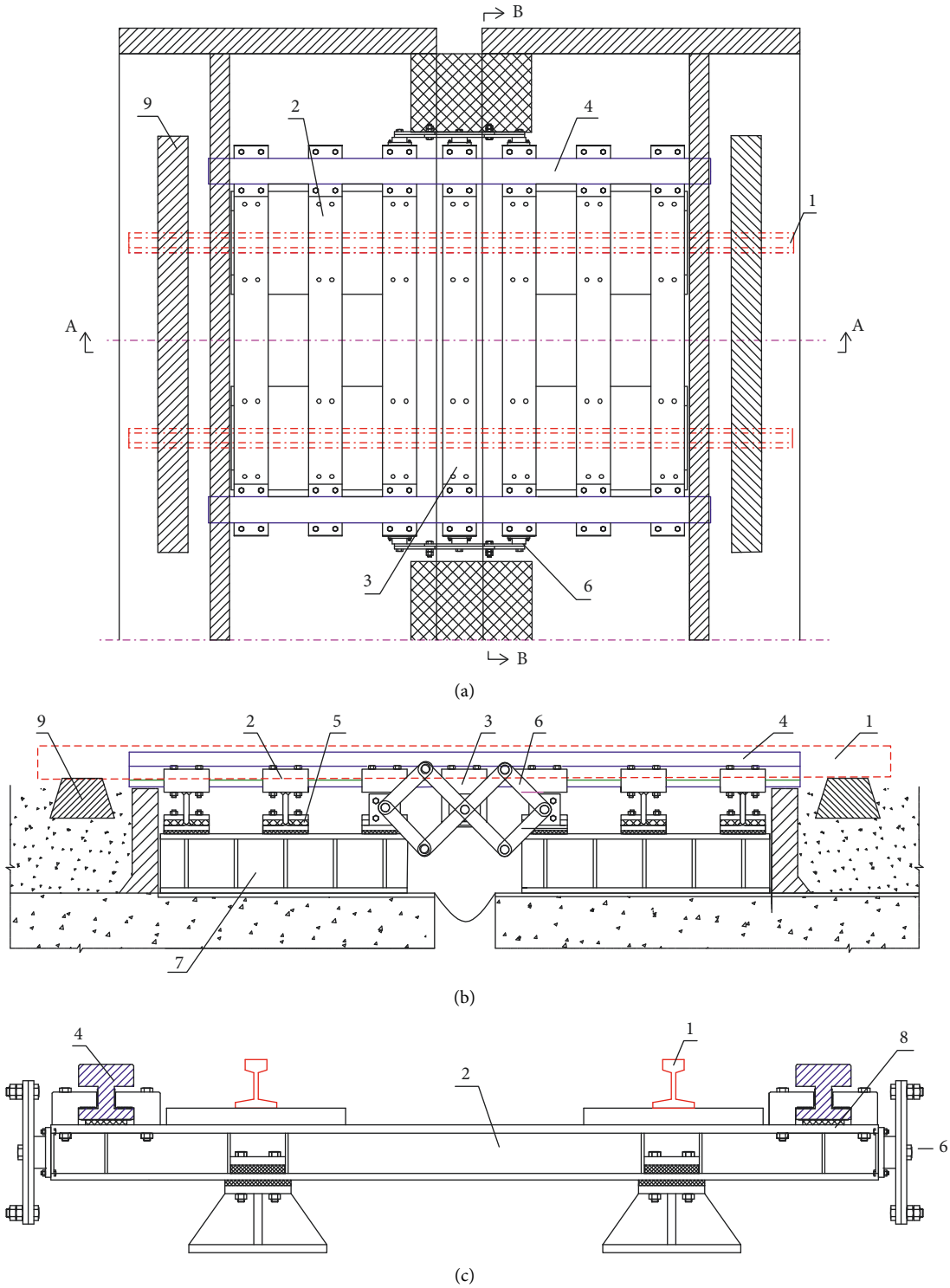

Figure 3: The structure of BEJs: (a) top view. (b) A-A section. (c) B-B section.

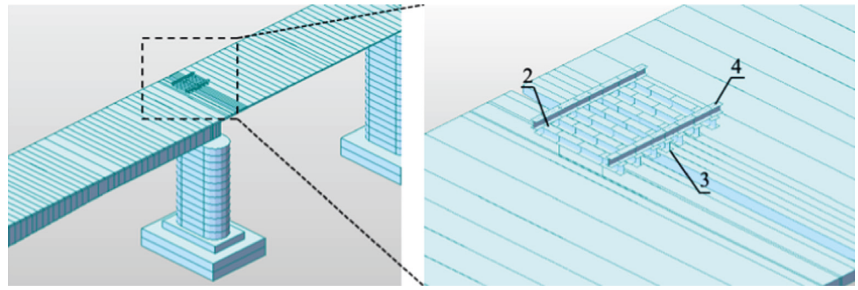

Figure 4: The MIDAS model of BEJs.

Table 1: Parameters of different cases.

Parameter	Case			
	1	2	3	4
Vertical stiffness of cushion plates (kN/mm)	80	120	80	120
Vertical stiffness of pressure-bearings (kN/mm)	160	160	240	240
Sleeper spacing (mm)	350, 450, 550			

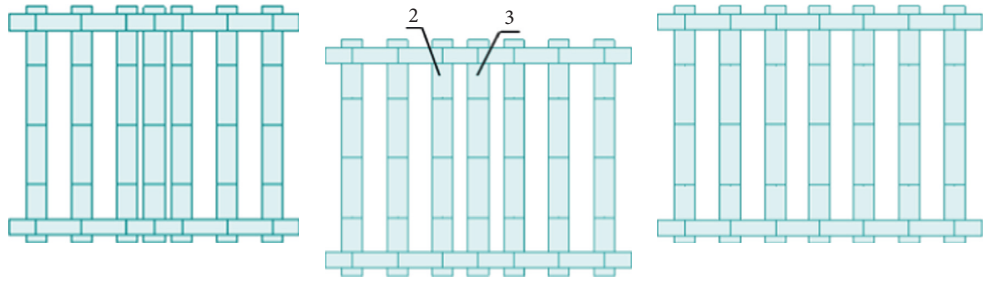

Figure 5: The top view of the BEJs model: (a) sleeper spacing is 350 mm, (b) 450 mm, and (c) 550 mm.

alignment irregularity, and cross-level irregularity, respectively; A_v and A_a is the constant of roughness; ω_r, ω_c, ω_s are the truncation frequency. The parameters are shown in Table 4.

$$S_v(\omega) = \frac{A_v\omega_c^2}{\left(\omega^2 + \omega_r^2\right)\left(\omega^2 + \omega_s^2\right)}, \tag{4}$$

$$S_a(\omega) = \frac{A_a\omega_c^2}{\left(\omega^2 + \omega_r^2\right)\left(\omega^2 + \omega_s^2\right)}, \tag{5}$$

$$S_c(\omega) = \frac{A_v\omega_c^2\omega^2}{\left(\omega^2 + \omega_r^2\right)\left(\omega^2 + \omega_c^2\right)\left(\omega^2 + \omega_s^2\right)}. \tag{6}$$

In this study, one specific rail irregularity sample is applied in all cases. When calculating the wheel-rail force in each step, wheel-rail relative displacement is superimposed on the track irregularity for calculation.

2.6. Vehicle-Track-Bridge Coupled Model. Vehicle, track, and bridge form a coupled system through the wheel-rail force and the interaction between the track and the bridge, the coupled model is shown in Figure 7. Equation (1)–(3) constitute the overall motion equation of the whole system. The equation is solved by the iterative method, and the specific solving process is shown in Figure 8.

3. Numerical Analysis

3.1. Dynamic Response of BEJs. Since the size and the mass of BEJs are much smaller than the bridge, the change of the BEJs' parameters has no effect on the dynamic response of the bridge. However, in order to show the dynamic response of BEJs more clearly, the results of the bridge are shown as a reference.

Figure 9 shows the maximum value of vertical displacement and acceleration of bridges and BEJs at different positions under Case 1 when sleeper spacing is 450 mm and the vehicle speed is 250 km/h. Since the limits in the code are given based on the maximum values, the values discussed in the paper are the maximum values. The horizontal ordinate represents the sequence that passed by the vehicle. It is shown that the dynamic response of bridges at different positions is basically the same. The dynamic response of BEJs at different positions is different, but it shows randomness,

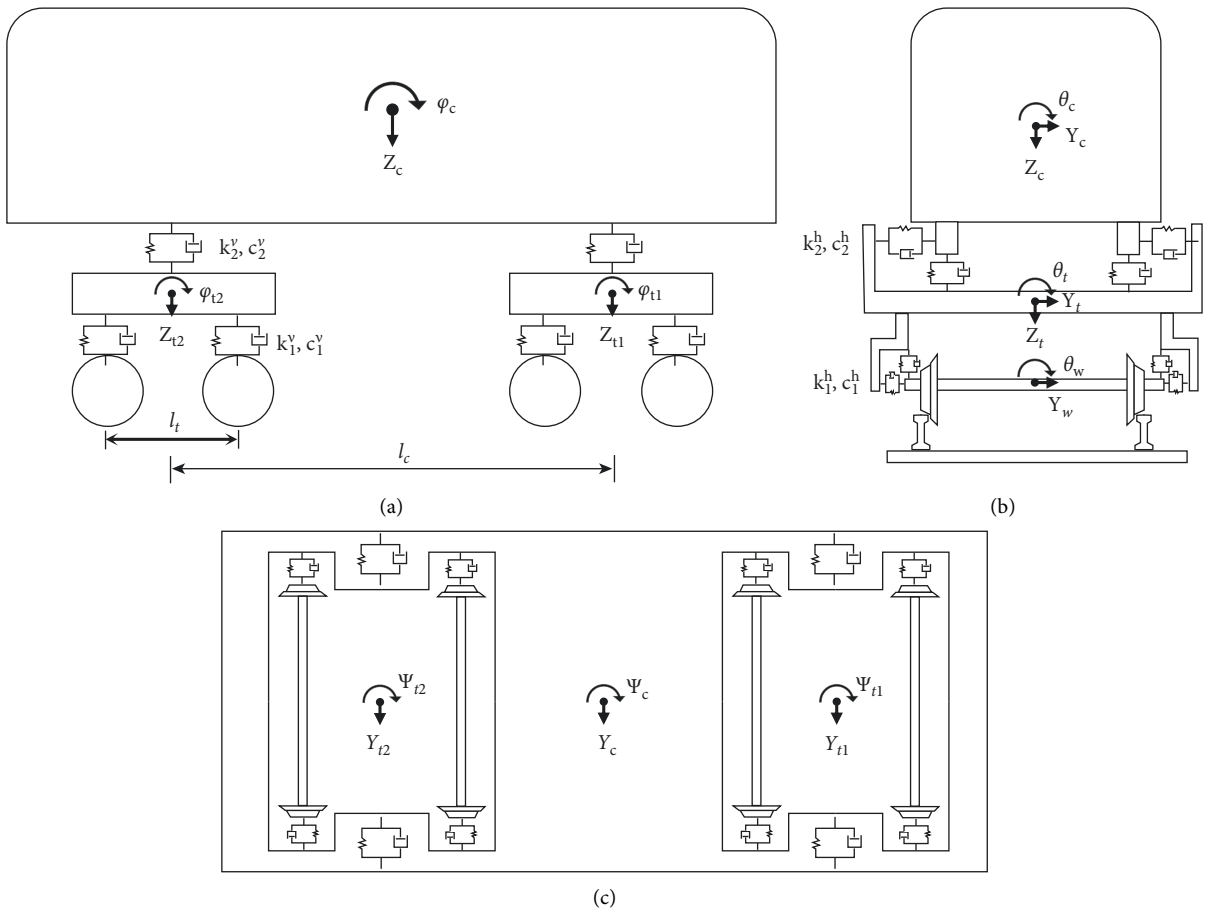

Figure 6: Vehicle model: (a) right view. (b) Rear view. (c) Bottom view.

Table 2: The main parameters of the vehicle model.

Parameters	Unit	Motor car/trailer car
Mass of car-body	kg	$3.96 \times 10^4/3.44 \times 10^4$
Mass of bogie	kg	$3.20 \times 10^3/2.60 \times 10^3$
Mass of wheelset	kg	$2.40 \times 10^3/2.40 \times 10^3$
Roll mass moment of the car-body	kg·m^2	$0.128 \times 10^6/0.111 \times 10^6$
Pitch mass moment of the car-body	kg·m^2	$1.94 \times 10^6/1.686 \times 10^6$
Yaw mass moment of the car-body	kg·m^2	$1.673 \times 10^6/1.453 \times 10^6$
Roll mass moment of the bogie	kg·m^2	$2.59 \times 10^3/2.106 \times 10^3$
Pitch mass moment of the bogie	kg·m^2	$1.752 \times 10^3/1.423 \times 10^3$
Yaw mass moment of the bogie	kg·m^2	$3.20 \times 10^3/2.60 \times 10^3$
Roll mass moment of the wheelset	kg·m^2	720/756
Lateral stiffness of the primary suspension system	kN/mm	$1 \times 10^3/1 \times 10^3$
Vertical stiffness of the primary suspension system	kN/mm	$1 \times 10^3/1 \times 10^3$
Lateral stiffness of the secondary suspension system	kN/mm	$0.2 \times 10^3/0.2 \times 10^3$
Vertical stiffness of the secondary suspension system	kN/mm	$0.2 \times 10^3/0.2 \times 10^3$
Lateral damping of the primary suspension system	kN·s/m	50/50
Vertical damping of the primary suspension system	kN·s/m	20/20
Lateral damping of the secondary suspension system	kN·s/m	50/50
Vertical damping of the secondary suspension system	kN·s/m	10/10
Distance of two bogies	m	17.5/17.5
Distance of two wheelsets	m	2.5/2.5

Table 3: The main parameters of the ballasted track.

Parameters	Unit	Value
Elastic modulus of rail	N/m^2	2.059×10^{11}
Inertia moment of rail cross section	m^4	3.217×10^{-5}
Mass of rail	kg/m	60.64
Spring stiffness of fastener	N/m	1×10^8
Damping coefficient of fastener	N/m	7.5×10^4
Spring stiffness of ballast	N/m	9.50×10^7
Damping coefficient of ballast	N/m	5.88×10^4

Table 4: The parameters of track irregularity PSD.

Parameter	ω_c (rad/m)	ω_r (Rad/m)	ω_s (rad/m)	A_a ($m^2 \cdot$ rad/m)	A_v ($m^2 \cdot$ rad/m)	A_g ($m^2 \cdot$ rad/m)
Value	0.8246	0.0206	0.4380	6.125×10^{-7}	10.08×10^{-7}	1.032×10^{-7}

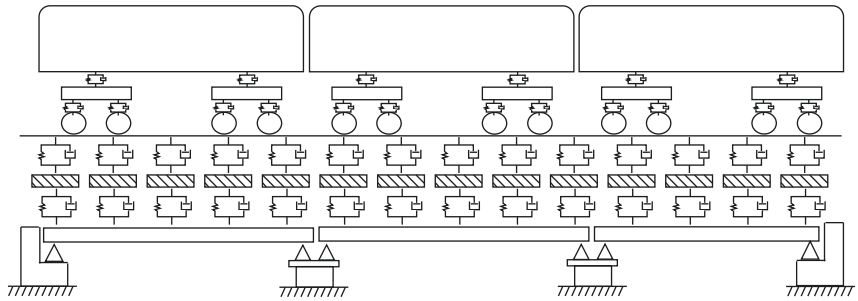

Figure 7: The model of the vehicle-track-bridge coupled system.

which may be related to the track irregularity and the state of vehicles passing by.

As the main part of BEJs, the supporting beam can be regarded as a continuous girder with fixed sleepers as support. Figure 10 shows the vertical dynamic response of the supporting beam of the third BEJs in time history in Case 1 when sleeper spacing is 450 mm and the vehicle speed is 250 km/h, and the dynamic response of midspan of the adjacent girder is shown as well. It can be seen that although the span of the supporting beam is much smaller than that of the bridge, its vertical displacement is close to that of the bridge. Therefore, BEJs is more likely to cause the deformation of under-track foundation with a small wavelength, and has a greater impact on running safety and stability. The vertical acceleration of the supporting beam is significantly greater than that of the bridge.

Figure 11 shows the vertical dynamic response of the movable sleeper, fixed sleeper, and supporting beam in the same BEJs in time history in Case 1 when sleeper spacing is 450 mm and the vehicle speed is 250 km/h. Since movable sleepers are only supported by the supporting beam, the vertical dynamic displacement of the movable sleeper is significantly greater than that of the fixed sleeper and the supporting beam. Similarly, the vertical accelerations of a movable sleeper are also greater than that of the fixed sleeper and the supporting beam.

Figure 12 shows the maximum values of the dynamic response of BEJs with different vehicle speeds in Case 1 when sleeper spacing is 450 mm. It can be seen that the dynamic response of BEJs increases with the increase of vehicle speed.

Figure 13 shows the vertical dynamic response of BEJs in time history in different cases when sleeper spacing is 550 mm and the vehicle speed is 250 km/h. It can be seen that the changing tendence of the dynamic response of the movable sleeper, fixed sleeper, and supporting beam are different when the vertical stiffness of BEJs changes. Figure 14 shows the maximum values of the dynamic response of BEJs under different cases when the vehicle speed is 250 km/h. The vertical displacement of the fixed sleeper is mainly affected by the vertical stiffness of the cushion plate. When the vertical stiffness of the cushion plate increases, the vertical dynamic displacement of the fixed sleeper decreases significantly. The vertical acceleration of fixed sleepers also shows the same trend. The stiffness change of pressure-bearing has no effect on the fixed sleeper. The vertical response of the movable sleeper is mainly affected by the vertical stiffness of pressure-bearing. When the vertical stiffness of pressure-bearing increases, the vertical dynamic displacement and vertical acceleration of the movable sleeper decrease significantly. With the increase of the vertical stiffness of the cushion plate, the vertical displacement of the movable sleeper decreases slightly. The vertical displacement of the supporting beam is mainly affected by the vertical stiffness of pressure-bearing. When the vertical stiffness of pressure-bearing increases, the vertical displacement of the supporting beam decreases significantly. The vertical stiffness of the cushion plate has

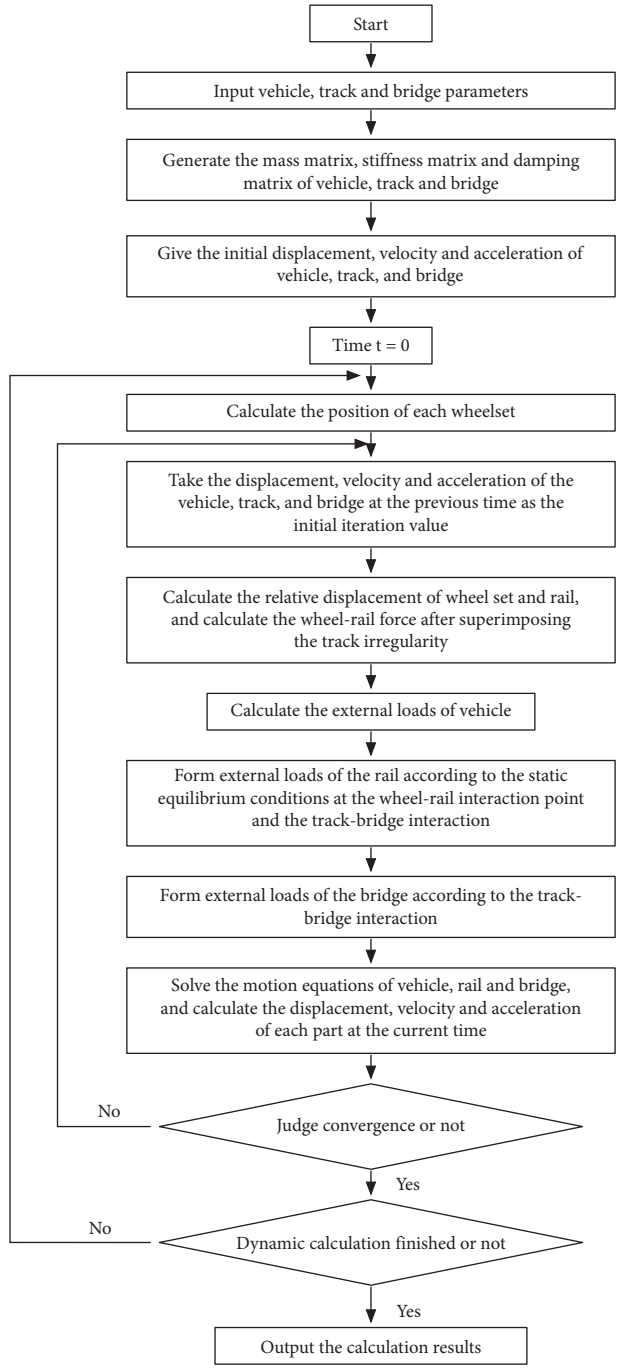

Figure 8: Solving process of the motion equation of the vehicle-track-bridge coupled system.

no effect on the vertical displacement of the supporting beam, but will affect the vertical acceleration of the supporting beam. When the stiffness of the cushion plate increases, the vertical acceleration of the supporting beam decreases significantly.

The dynamic response of BEJs is also affected by sleeper spacing. Although the changing trend of each part is different, in general, when sleeper spacing is the largest, the dynamic response of BEJs is also the largest.

According to the regulation TB 10761–2013 (technical regulations for dynamic acceptance for high-speed railways construction) [24], the vertical displacement of the sleeper should not exceed 2 mm, and the vibration acceleration of the sleeper should not exceed 500 m/s^2. When the stiffness of pressure-bearing is 160 kN/mm and sleeper spacing is 550 mm, the vertical displacement of the movable sleeper will exceed the limit, which may affect the running safety. Based on the results of BEJs, the larger vertical stiffness of pressure-bearing is recommended.

3.2. Dynamic Response of the Vehicle. According to the specification GB5599-2019 (specification for dynamic

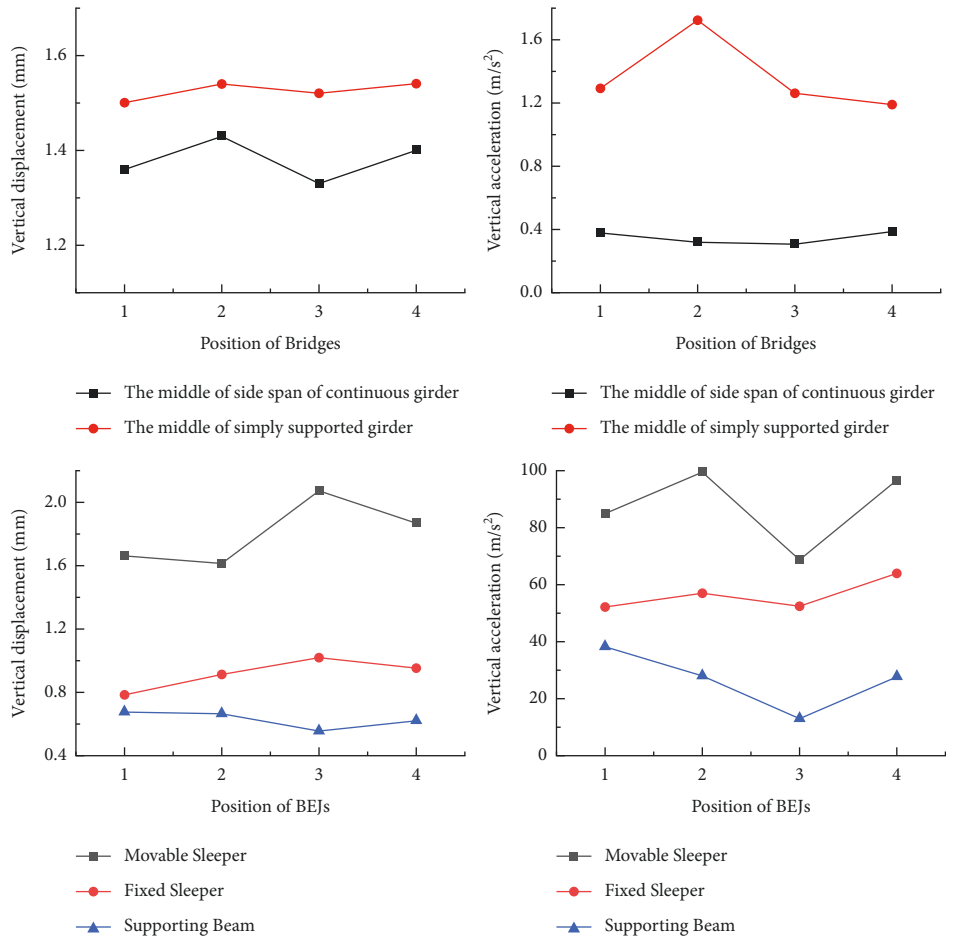

Figure 9: The maximum value of vertical dynamic response of BEJs and bridges at different positions in Case 1.

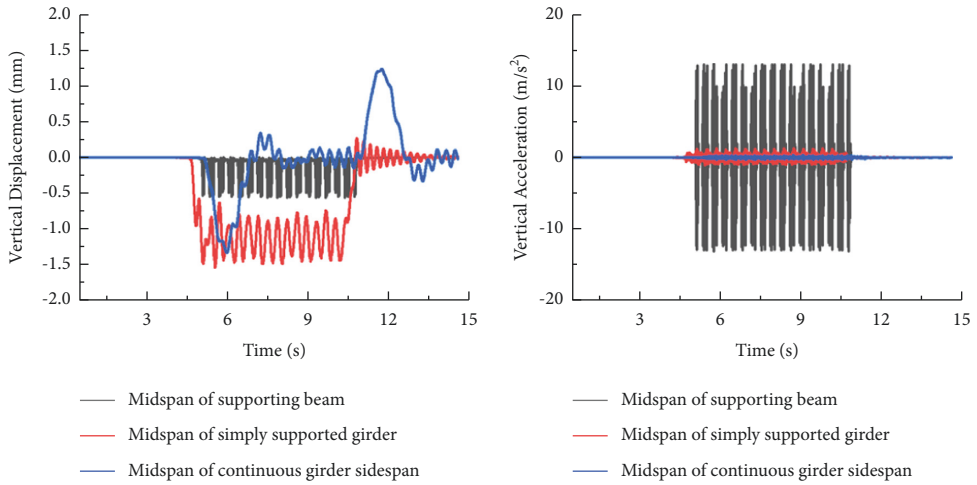

Figure 10: Time histories of the vertical dynamic response of BEJs and bridges adjacent to BEJs in Case 1.

performance assessment and testing verification of the rolling stock) [25], the dynamic response of the vehicle is evaluated by safety indexes and stability indexes: derailment factor Q/P, wheel unloading rate $\Delta P/\overline{P}$, the lateral wheel-rail force Q, vertical vibration acceleration of the car-body α_z, lateral vibration acceleration of the car-body α_y, and the Sperling index of comfort W in the vertical direction and lateral direction, while P represents the vertical wheel-rail force, ΔP represents the offload vertical wheel-rail force, $\overline{P}$ represents the average static vertical wheel-rail force, and W is the frequency weighted value of acceleration of the car-body. The allowable values of indexes are listed in Table 5.

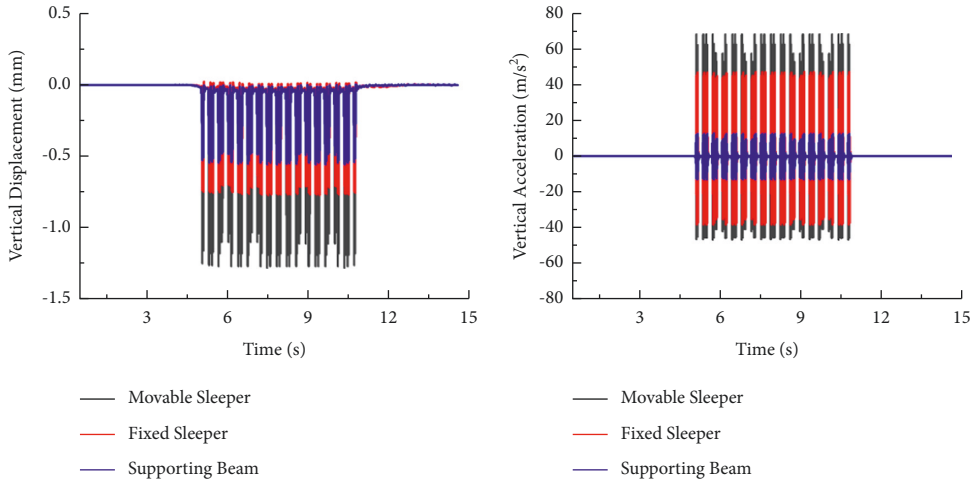

Figure 11: Time histories of the vertical dynamic response of BEJs in Case 1.

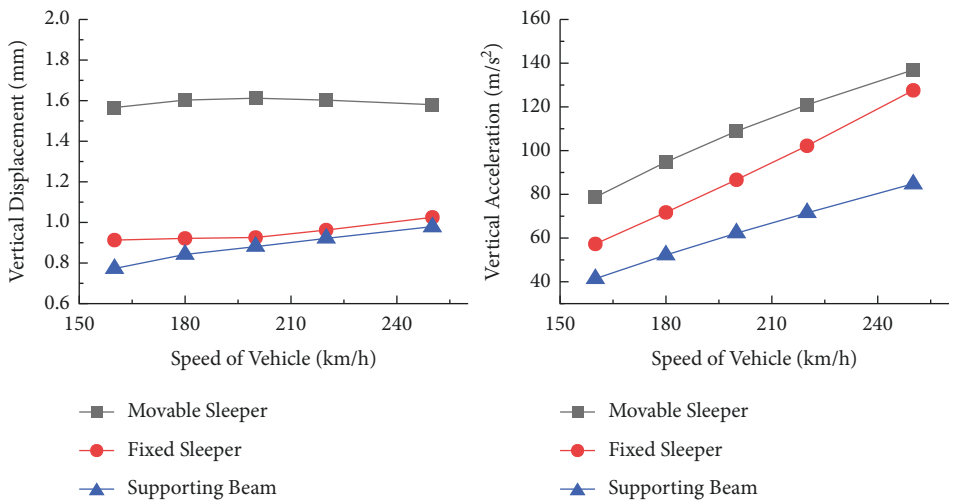

Figure 12: The maximum value of dynamic response of BEJs with different vehicle speed in Case 1.

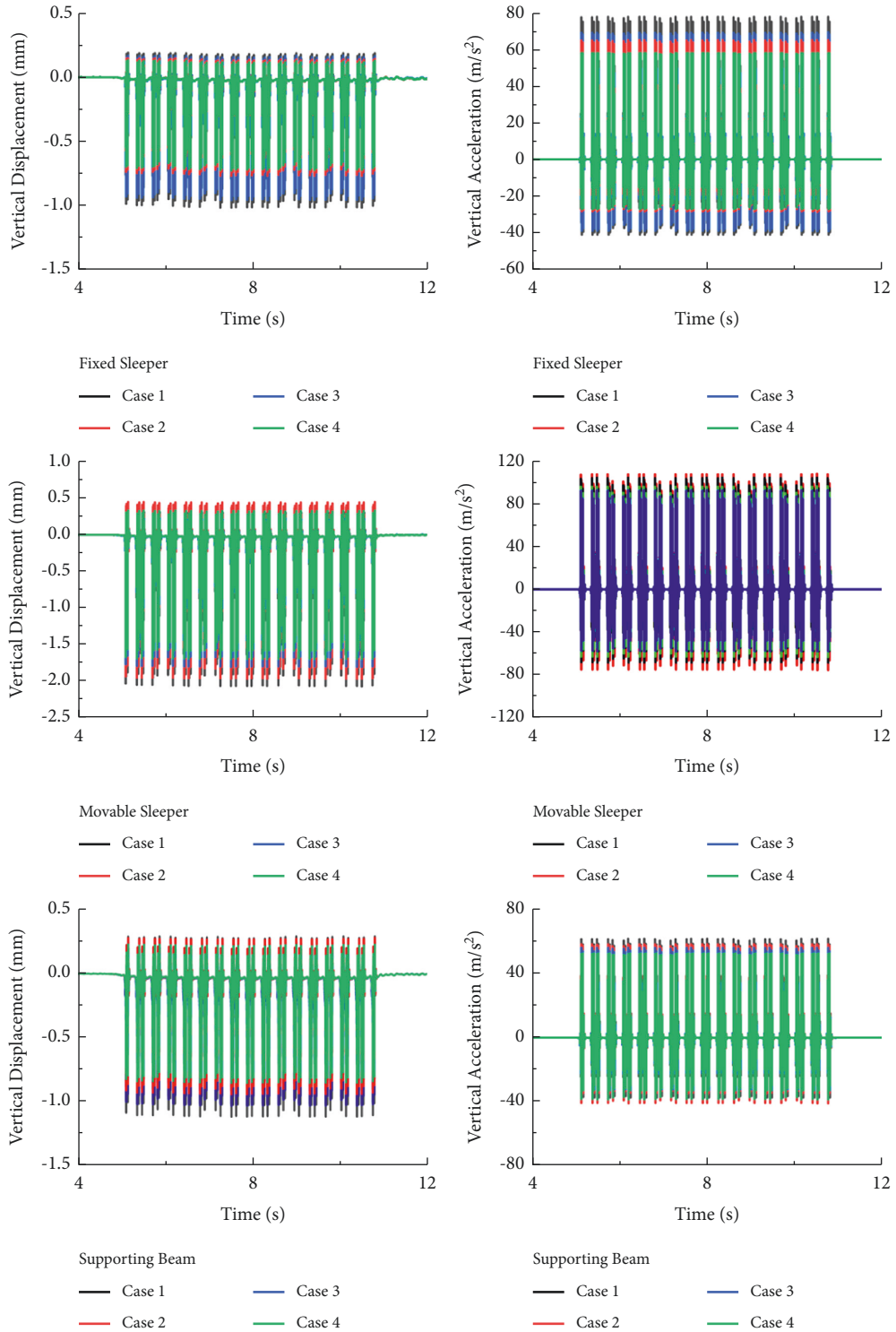

Figure 13: Time histories of the dynamic response of BEJs in different cases.

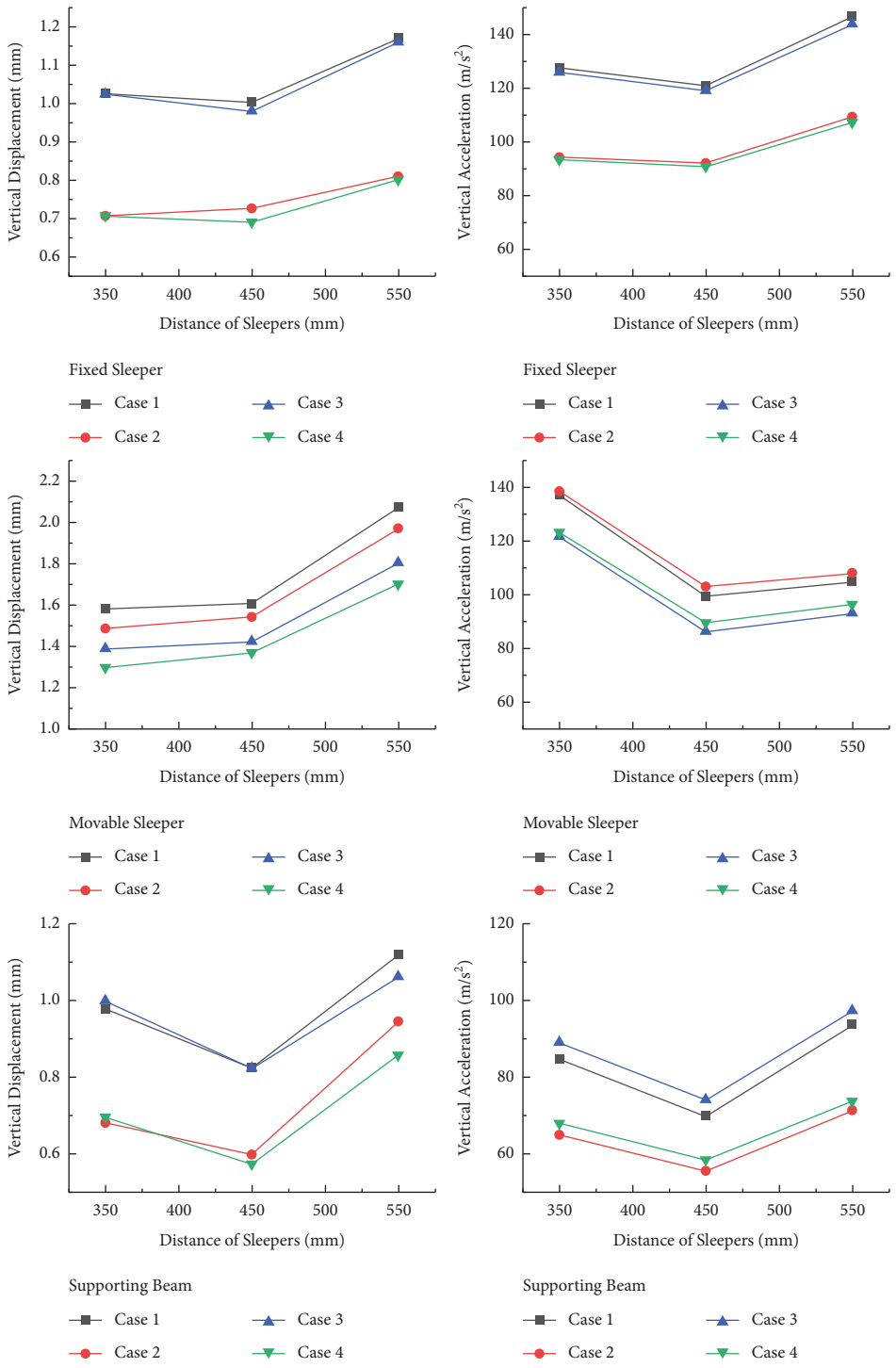

Figure 14: The maximum value of the dynamic response of BEJs in different cases.

Table 5: Allowable values of evaluation indexes of the vehicle.

Index	Q/P	$\Delta P/\overline{P}$	Q (kN)	α_z	α_y	W_z W_y
Allowance value	≤ 0.8	Qualified: ≤ 0.6 Dangerous: ≤ 0.65	≤19 + 0.3P	≤ 0.13 g	≤ 0.1 g	Excellent: ≤2.5 Good: 2.5 ~ 2.75 Qualified: 2.75 ~3 .0

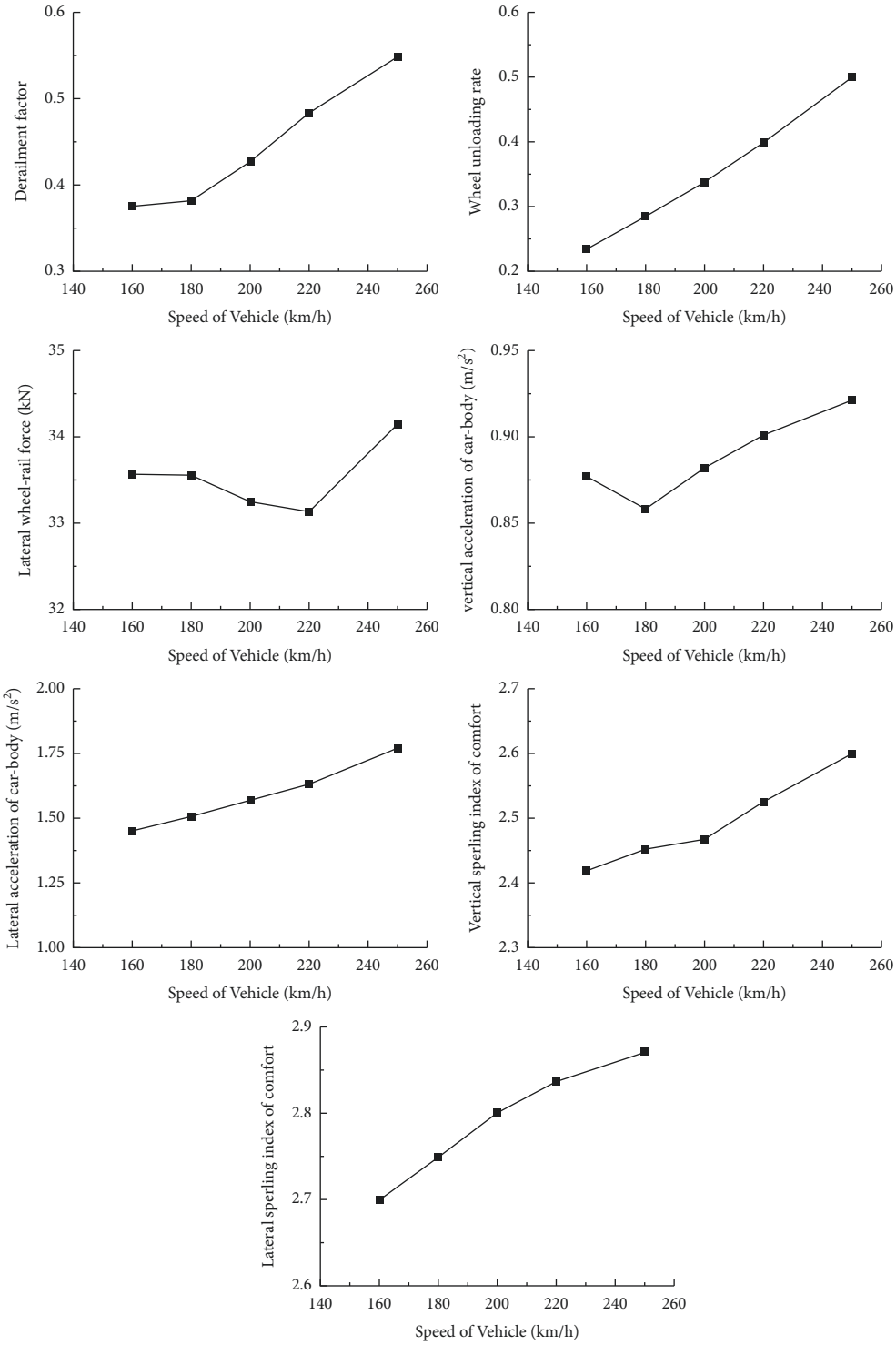

Figure 15: The maximum value of evaluation indexes of the vehicle with different speed in Case 1.

Table 6: Evaluation indexes of the vehicle in different load cases.

Load case	Sleeper spacing (mm)	Q/P	$\Delta P/\overline{P}$	Q (kN)	α_z (m/s^2)	α_y (m/s^2)	W_z	W_y
1	350	0.548	0.499	34.14	0.921	1.769	2.598	2.87
1	450	0.548	0.550	34.193	0.921	1.764	2.603	2.882
1	550	0.548	0.585	34.147	0.921	1.769	2.603	2.873
2	450	0.548	0.476	34.193	0.921	1.764	2.568	2.883
3	450	0.548	0.544	34.193	0.921	1.764	2.603	2.882
4	450	0.548	0.476	34.193	0.921	1.764	2.568	2.883

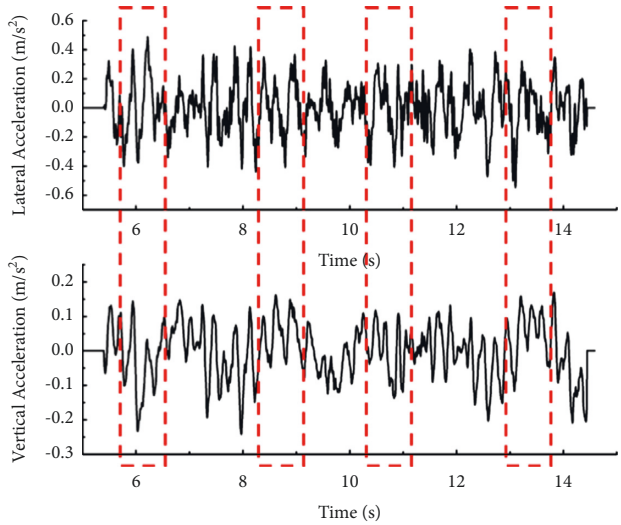

Figure 16: Time histories of acceleration of the last car-body in Case1.

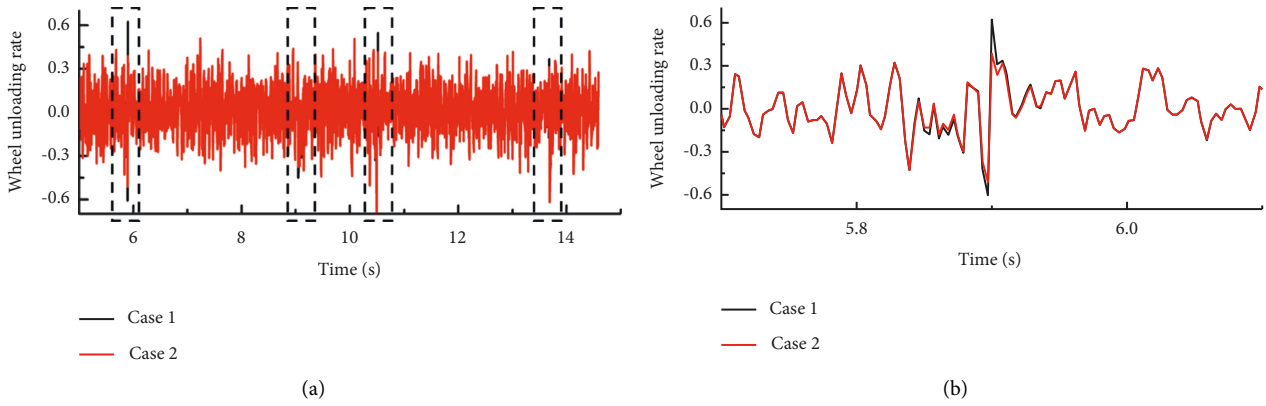

Figure 17: Time histories of the wheel unloading rate of the last wheelset in different cases: (a) the whole time period (b) the time period when the wheelset passes the first BEJs.

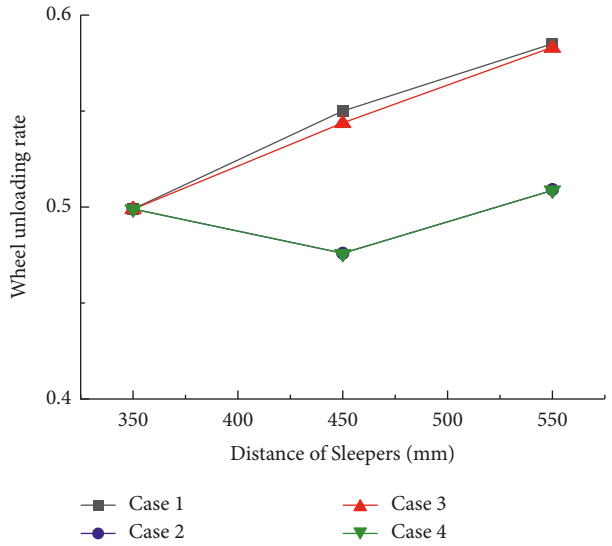

Figure 18: The maximum value of the wheel unloading rate in different cases.

The changes of indexes with the different speed of the vehicle in load Case 1 are shown in Figure 15, while sleeper spacing is 450 mm. It can be seen that all evaluation indexes of the vehicle become worse when the speed of vehicle increases.

Table 6 lists the maximum values of evaluation indexes under different cases at the vehicle speed of 250 km/h. On the whole, the evaluation indexes of the vehicle under different load cases meet the specification. The evaluation indexes of the vehicle are almost the same in different load cases, except the wheel unloading rate.

Figure 16 shows the vertical and lateral acceleration of the last car-body in time history in Case 1 when sleeper spacing is 550 mm and the vehicle speed is 250 km/h, and the red boxes indicate the positions of the four BEJs. Due to the cushioning of the vehicle, BEJs has no obvious effect on the acceleration of the car-body, but will affect the interaction between the wheelset and the rail. Figure 17 shows the wheel unloading rate of the last wheelset in time history. It can be seen that the wheel unloading rate on BEJs will be greater than that on the bridge. The wheel unloading rate of the vehicle only changes with the stiffness of BEJs when the vehicle passing through BEJs. As shown in Figure 18, the influence of the vertical stiffness of the cushion plate on the wheel unloading rate is more obvious than that of pressure-bearing. The increase of vertical stiffness of the cushion plate will significantly reduce the wheel unloading rate. It is worth noting that the wheel unloading rate is close to the limit value 0.6 when sleeper spacing is 550 mm in load Case 1 and 3. It indicates that the wheel unloading rate may exceed the limit if the vertical stiffness of the cushion plate is insufficient. Therefore, the larger vertical stiffness of the cushion plate is recommended.

4. Conclusion

This study investigated the influence of the parameters of BEJs on the dynamic response of the vehicle-track-bridge coupled system. A three-dimensional vehicle-track-bridge model is established, in which the vehicle is modeled by multibody dynamics, and the track and bridges are modeled by the finite element method. The dynamic response of the system when the vehicle passes through the railway line with densely arranged BEJs is calculated by the iterative method, and the effect of vehicle speed and sleeper spacing are taken into consideration.

The main conclusions of this study are:

(1) The vertical stiffness of BEJs will affect the interaction between the wheel and the rail. The wheel unloading rate may exceed the limit of specification when the vertical stiffness of the cushion plate is insufficient.

(2) The movable sleeper is the most noteworthy part of BEJs because the movable sleeper is suspended. When the vertical stiffness of pressure-bearing is insufficient, the vertical displacement of the movable sleeper will exceed the limit of regulation, which will hurt the running safety.

(3) The dynamic response of BEJs and the vehicle is affected by the vehicle speed and sleeper spacing. With the increase of vehicle speed and sleeper spacing, the dynamic response of BEJs and the vehicle increases.

The influence of the vertical dynamic stiffness of BEJs on the dynamic response of the vehicle-track-bridge coupled model is clarified in this study. And this study provided a theoretical basis for adopting the stiffness of BEJs by analyzing the dynamic response of the vehicle and BEJs. Based on the research results, the larger vertical stiffness of the cushion plate and pressure-bearing is recommended. The results have been applied to the design of BEJs on the studied railway line, which are in good service condition at present.

Due to the complexity and the diversity of BEJs in different bridges, the influence of BEJs on the running safety and stability will be further studied in our future work.

Data Availability

The data used to support the findings of this study are available from the corresponding author upon request.

Conflicts of Interest

The authors declare that there are no conflicts of interest regarding the publication of this paper.

Acknowledgments

This research project was financially supported by the (1) National Natural Science Foundation of China under Grant no. U1934207; (2) China State Railway Group Co., Ltd. under Grant no. SY2021G002; (3) China Academy of Railway Sciences Co., Ltd. under Grant no. 2021YJ258; and (4) Infrastructure Inspection Research Institute of China Academy of Railway Sciences Co., Ltd. under Grant no. 2021JJXM08.

References

[1] M. Gao, G. Li, and F. Yang, "Vertical coupling dynamic analysis method and engineering applications of vehicle-track-substructure based on forced vibration," *China Railway Science*, vol. 42, no. 2, pp. 50–58, 2021.

[2] T. Arvidsson, A. Andersson, and R. Karoumi, "Train running safety on non-ballasted bridges," *International Journal of Reality Therapy*, vol. 7, no. 1, pp. 1–22, 2019.

[3] W. Zhai and H. Xia, "High-speed train-track-bridge dynamic interactions - Part I: theoretical model and numerical simulation," *International Journal of Reality Therapy*, vol. 1, no. 1-2, pp. 3–24, 2013.

[4] M. Gao and J. Pan, *The Dynamic Analysis of Vehicle-Track-Railway Bridge System*, China Railway Publishing House, China, 2008.

[5] J. Yang, J. Sun, and M. Gao, "Vehicle-bridge coupling analysis for reverse curve MIxed passenger and freight railway bridge," *China Railway Science*, vol. 40, no. 2, pp. 46–53, 2019.

[6] G. Li, G. Li, and M. Gao, "Analysis of train-track dynamic behavior in bridge-tunnel transition section considering temperature deformation of CRTS I slab ballastless track," *Railway Engineering*, vol. 58, no. 1, pp. 133–137, 2018.

[7] N. Zhang, Z. Zhou, and Z. Wu, "Safety evaluation of a vehicle-bridge interaction system using the pseudo-excitation method," *Railway Engineering Science*, vol. 30, no. 1, pp. 41–56, 2022.

[8] L. Jiang, X. Liu, P. Xiang, and W. Zhou, "Train-bridge system dynamics analysis with uncertain parameters based on new point estimate method," *Engineering Structures*, vol. 199, Article ID 109454, 2019.

[9] W. Gong and Z. Zhu, "Running safety assessment of a train traversing a three-tower cable-stayed bridge under spatially varying ground motion," *Railway Engineering Science*, vol. 28, no. 2, pp. 184–198, 2020.

[10] P. Xiang and M. Wei, "Creep effect on the dynamic response of train-track-continuous bridge system," *International Journal of Structural Stability and Dynamics*, vol. 21, no. 10, Article ID 2150139, 2021.

[11] Z. Chen, "Relationship between track stiffness and dynamic performance of vehicle-track-bridge system," *Vehicle System Dynamics*, vol. 59, no. 12, pp. 1825–1843, 2020.

[12] L. Chen and Y. Lee, "Evaluation of performance of bridge deck expansion joints," *Journal of Performance of Constructed Facilities*, vol. 16, no. 1, pp. 3–9, 2002.

[13] B. Zuada Coelho and A. Vervuurt, "Dynamics of modular expansion joints: the martinus nijhoff bridge," *Engineering Structures*, vol. 48, no. Mar, pp. 144–154, 2013.

[14] E. Mccarthy and T. Wright, "Development of an experimentally validated analytical model for modular bridge expansion joint behavior," *Journal of Bridge Engineering*, vol. 19, no. 2, pp. 235–244, 2014.

[15] Y. Ding, W. Zhang, F. Au, and F. T. Au, "Effect of dynamic impact at modular bridge expansion joints on bridge design," *Engineering Structures*, vol. 127, pp. 645–662, 2016.

[16] Z. Sun and Y. Zhang, "Failure mechanism of expansion joints in a suspension bridge," *Journal of Bridge Engineering*, vol. 21, no. 10, Article ID 05016005, 2016.

[17] L. Deng, W. Yan, and Q. Zhu, "Vehicle impact on the deck slab of concrete box-girder bridges due to damaged expansion joints," *Journal of Bridge Engineering*, vol. 21, no. 2, Article ID 06015006, 2016.

[18] P. Xiang, W. Huang, and L. Jiang, "Investigations on the influence of prestressed concrete creep on train-track-bridge system," *Construction and Building Materials*, vol. 293, Article ID 123504, 2021.

[19] W. Zhai, "Vehicle-Track Coupled Dynamics," The Science Publishing Company, China, 2018.

[20] W. Zhai, Z. Han, and Z. Chen, "Train-track-bridge dynamic interaction: a state-of-the-art review," *Vehicle System Dynamics*, vol. 57, no. 7, pp. 984–1027, 2019.

[21] H. Xia, W. Guo, and N. Zhang, "Dynamic analysis of a train-bridge system under wind action," *Computers & Structures*, vol. 86, no. 19-20, pp. 1845–1855, 2008.

[22] J. Yang, N. Zhang, and H. Xia, "Comparative analysis on applicability of four wheel-rail vertical contact models for coupling vibration of vehicle-track system," *China Railway Science*, vol. 37, no. 6, pp. 11–20, 2016.

[23] H. Xia and N. Zhang, *Dynamic Interaction of Vehicles and Structures*, The Science Publishing Company, China, 2005.

[24] People's Republic of China National Railway Administration, *Technical Regulations for Dynamic Acceptance for High-Speed Railways Construction*, People's Republic of China National Railway Administration, Beijing, China, 2013.

[25] People's Republic of China National Railway Administration, *Specification for Dynamic Performance Assessment and Testing Verification of Rolling Stock*, People's Republic of China National Railway Administration, Beijing, China, 2019.